

# An Effective Method for Data Processing of Inertial Measurement Units Applied to Embedded Systems

Christoph Kolhoff<sup>a</sup> and Markus Kemper

ZME-Institute, UAS Diepholz (PHWT), Thüringer Str. 3a, Diepholz, Germany

**Keywords:** Bias Error, Gauss-Markov Process, MEMS Error Model.

**Abstract:** Autonomous functions for navigation and localization have piqued the attention and interest in many fields of science and engineering as automotive, aviation and robotics. Desiring high quantity of autonomous products, the used components are requested to be cheap. This often lead engineers or developers to apply micro-electromechanical systems that exhibit large errors. To use these sensors anyway, the acquired data must be processed online for error reduction. Hence there is a need for an algorithm that is easy to compute. The aim of this research is to develop a generic algorithm based on a Gauss-Markov process representing the drifting bias that can be parametrized easily and performs well on real-time systems. Therefore, the error model imitates the sensor's output and removing the errors afterwards. Finally, a validation of the suggested algorithm is performed by comparing processed data of the micro-controller to data processed a posteriori on a high-performance computer.

## 1 INTRODUCTION

Autonomous functions are designed to make decisions based on data acquired from sensors without any human assistance. In foreseeable future autonomous devices are purposed to take tasks in various sections of daily life which requires a large large amount of several accurate sensor data. The commonly used sensors deliver those precise data but they lead to high costs of the final product. For low-cost robotic systems on customer markets the used sensors are requested to be cheap on the one hand and have to provide data with small errors on the other hand. Hence, micro-electromechanical systems (MEMS) are the point of interest in many cases. These kind of sensors exhibit large tolerances and wide ranges of errors as shown in (Kolhoff et al., 2021). In (Titterton and Weston, 2004) an error model for triaxial IMUs is given to describe the connectedness between the real and the measured values. This model contains both, repeatable (e.g. misalignment, scaling errors, static bias) and non repeatable (e.g. noise) effects. Looking at (Titterton and Weston, 2004), it is recommended to compensate only repeatable errors by applying the chosen error model. Processing stochastic effects is not considered by this approach. Acquired data have to be processed in "real time" to improve their quality

and to reduce errors which leads to the need for sufficient algorithms. Concerning automotive application, inertial measurement units (IMUs) consisting of accelerometers and gyroscopes are focused to determine the relevant properties of the vehicle's actual motion. To take account of these requirements, the mathematical structure of the sensor's behavior has to be known to be able to develop an algorithm for data processing. Therefore, an easy model containing misalignment, constant and drifting bias, noise and nonlinear effects in triads of sensors is given by (Kuncar et al., 2018). Additionally, in (Gebre-Egziabher, 2004) some methods are presented to identify the needed parameters easily. As a further important requirement, the model is not just purposed to be parametrized for only one specific sensor, but for an entire class of sensors. In this paper the bias is the focused kind of error because of its long-time drift characteristics.

In known applications the static component of the bias is considered only and therefore the entire bias cannot be compensated completely. Especially when an integration over time is performed (e.g. by determining the orientation from the angular velocity), the resulting errors rise very quickly with time as shown in (Ramalingam et al., 2009). To design an algorithm meeting these requirements, the drift of the sensor's bias is approximated by a first order Gauss-Markov process (GM) for a single axis, referring to (Gebre-

<sup>a</sup>  <https://orcid.org/0000-0002-7880-8152>



Figure 1: Autonomous "People-Mover"-Project at UAS Diepholz.

Egziabher, 2004). In addition to this, the model is extended by integrating the drifting bias and the algorithm is implemented on a micro-controller afterwards. Finally, the processed data of the micro-controller are compared to the same data filtered by the suggested algorithm on a high-performance computer. It is shown that the mentioned errors are strongly reduced by the suggested algorithm and the algorithm is sufficient to operate on real-time systems. At UAS Diepholz, a fully autonomous low-cost "People-Mover" is developed. Figure (1) shows a photograph while testing sensor systems. The car is based on an e.Go-Cart and is equipped with sensors and actuators for self-driving modes. The maximum speed is 25 to 45 kilometers per hour. Hence, in this paper, an effective method for data processing of Inertial Measurement Units for the application in low-cost autonomous systems is proposed.

## 2 THEORETICAL BACKGROUND

### 2.1 Generic Error Model for IMUs

The considered sensors exhibit various kinds of errors. Referring to (Titterton and Weston, 2004) a generic error model for triads of accelerometers and gyroscopes is denoted in (1) connecting the vector of measured values  $\tilde{\mathbf{x}}$  and real values  $\mathbf{x}$ . The model contains errors, e.g. due to misalignment represented by the matrix  $\mathbf{M}$ .

$$\tilde{\mathbf{x}} = \mathbf{M} \cdot \mathbf{x} + \mathbf{x}_b + \mathbf{x}_p + \mathbf{x}_{nl} \quad (1)$$

This type of error is caused by faulty assembling of the sensor on the one hand and a lack of orthogonality of the three sensing axes of the IMU resulting from imperfections in the production process on the other hand. This is depicted in Figure 2. The accelerations and angular velocities appear along the solid axes which are aligned orthogonally to each other.

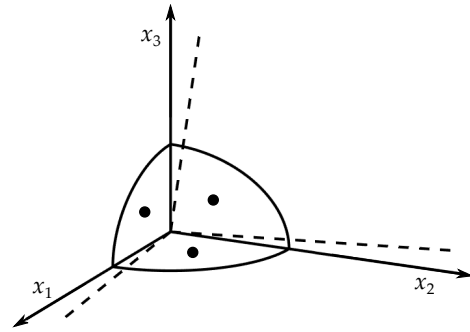


Figure 2: Misalignment of the sensor's axes.

The sensor measures values along the dashed axes. Due to the non-orthogonal alignment of the IMU's axes the measured values contain amounts of the values of all solid axes and therefore they appear as linear combinations of all solid axes' values. Another reason for this behavior is a fault of sensitivity of each axis caused by errors in the production process. Elements of the major diagonal differing from a value of one represent errors in sensitivity of the respective axis. This is caused by the inclination of the dashed axes to the solid axes. Furthermore, the inclination leads to the fact that values measured along the dashed axes contain amounts of values that are measured along the other two solid axes. This is represented by the minor diagonal elements of  $\mathbf{M}$  which have commonly small magnitudes (Unsal and Demirbas, 2012). The measured values in this case lead to the assumption that accelerations and angular velocities occur on axes of the solid coordinate system in Figure 2 even if there are none in reality. A further component of the error model is the bias  $\mathbf{x}_b$ . Due to affection of gravity and imperfections of the internal structure of the sensor a constant bias  $\mathbf{x}_{b,stat}$  is the first part of  $\mathbf{x}_b$ . Because MEMS have to be powered externally, the electric conduction causes heating of the sensor (Wüstling, 1997). Due to this the internal geometry of the sensor is diversified and the bias drifts over time. This is considered by  $\mathbf{x}_{b,drift}$ , the second part of  $\mathbf{x}_b$ . As many other sensors MEMS exhibit noise  $\mathbf{x}_p$  which is assumed as zero-mean white noise with variance  $\sigma_w^2$  and a band-limit much higher than the relevant frequencies. The last type of errors is reasoned by nonlinear effects  $\mathbf{x}_{nl}$  that occur at high accelerations and angular velocities (Wüstling, 1997).

### 2.2 Characteristics of the Bias

As mentioned in (Ramalingam et al., 2009) and (Gebre-Egziabher, 2004) the bias  $b$  of a sensor contains a constant component  $b_0$  and a component  $b_1$  varying with time  $t$  as shown in (2) for each axis of

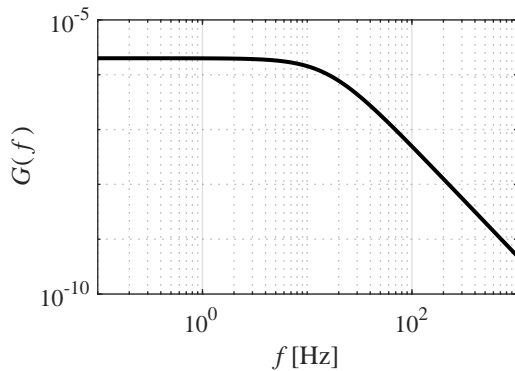


Figure 3: Power spectral density of a Gauss Markov process.

the triaxial sensor.

$$b(t) = b_0 + b_1(t) \tag{2}$$

From the beginning of long-time measured values the parameter  $b_0$  is determined easily, whereas the characterization of  $b_1$  is often more challenging. As shown from experimental data in (Kolhoff et al., 2021),  $b_1$  can be assumed as exponentially shaped. Looking at (Gebre-Egziabher, 2004), (Rasmussen and Williams, 2006) and (Brown and Hwang, 2012), a very simple method for modeling the drifting bias with constant ambient temperature is a continuous first order Gauss-Markov process (GM)  $g$  defined by the differential equation shown in (3).

$$\dot{g}(t) = -T_c^{-1} \cdot g(t) + w_g \quad \text{with} \quad g(0) = 1 \tag{3}$$

Herein,  $T_c$  is the correlation time of the process and  $w_g$  is the Gaussian driving process noise with variance  $\sigma_g^2$ . The magnitude of the drifting bias is determined from the end and the beginning of long-time measured values. Looking at (Brown and Hwang, 2012), this method is a stationary one fitting well to processes that exhibit long correlation times. Due to the stochastic component the process is not deterministic. The stochastic component  $w_g$  is neglected at first to show the general concept of determining  $T_c$  for a denoised process. Therefore, the auto-correlation function (ACF)  $\Phi$  is computed from denoised  $g$  as shown in (Gelb et al., 2001). The solution is shown in (4) with its maximum  $A^2$  at time lag  $\tau = 0$ .

$$\Phi(\tau) = \int_{-\infty}^{\infty} g(t) \cdot g(t + \tau) dt = A^2 \cdot \exp(-T_c^{-1} \cdot |\tau|) \tag{4}$$

All correlation values with a time lag different from zero are smaller than without time lag due to the ACF's exponential shape. This results in decreasing correlation between samples with increasing time lag (Brown and Hwang, 2012). Concerning (Gelb et al., 2001),  $T_c$  is identified from a time series of measured

noisy data by the point when the ACF has decayed to  $\exp(-1)$  (approximately 36.8 percent) of its maximum. As to that, when one is able to compensate the constant and the time-dependent drift of the sensor, only stochastic effects, scaling errors and cross-axes-effects will be left.

$$G(f) = \frac{2 \cdot A^2 \cdot T_c^{-1}}{(2j \cdot \pi \cdot f)^2 + T_c^{-2}} \tag{5}$$

A further need to ensure the usability of the GM for slowly drifting processes is to look at its power spectral density function (PSD)  $G$  with frequency  $f$ . This can be done best by computing the Fourier-Transformation of its ACF which leads to the PSD shown in (5), referring to (Lamon, 2018). The corresponding graph is shown in Figure 3 for  $T_c = 10$  milliseconds and  $A = 1$ . When looking at the plot it can be seen that the GM's energy is concentrated at low frequencies. Therefore, this model can be used to describe processes that differ slowly related to its characteristic values as mentioned in (Brown and Hwang, 2012).

### 2.3 Moving Average Smoothing

For data smoothing the moving average (MA) method is introduced in (Hyndman, 2010) and (Smith, 1999). It computes the average  $\hat{z}$  for a time index  $l$  from a connected set of  $n$  values from time series  $z$ . There are two versions to use the moving average. One is to use the two-sided version which means, that the set contains data before and after the current time index that the moving average is computed for. At this, the number of samples before and after the current time index can be chosen equally or different, resulting in a symmetrically or asymmetrically two-sided moving average. When concerning real-time applications, only data from previous points of time can be used for further processing. This version is called one-sided moving average, its calculation is shown in (6). Herein it becomes clear, that the oldest value is

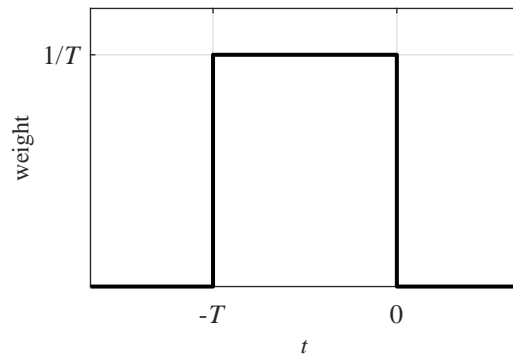


Figure 4: Moving Average filter.

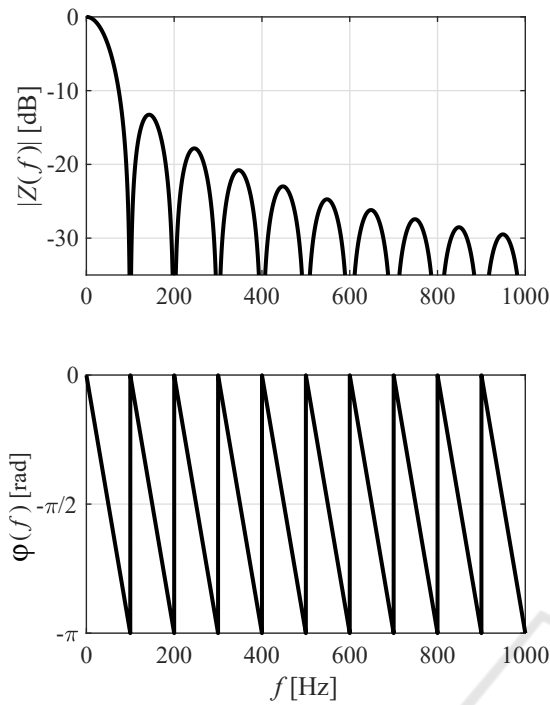


Figure 5: Bode plot for a Moving Average filter.

dropped and a new one is added to the set before computing the moving average for the new time index.

$$\hat{z}(l) = \sum_{k=0}^{n-1} a_k \cdot z_{l-k}, \quad l \in [k+1, n-1], \quad a_k = n^{-1} \quad (6)$$

The filter function in continuous time domain is shown in Figure 4. Due to the computation from past values, the use of the moving average causes a phase delay as shown in (Roscoe and Blair, 2016). In common applications all considered values are weighted equally so the ideal moving average filter is a Finite Impulse Response (FIR) filter with duration  $T$  and height  $\frac{1}{T}$ . Transforming (6) into Laplace domain leads to (7).

$$Z(s) = \frac{1}{T \cdot s} \cdot (1 - e^{-T \cdot s}) \quad (7)$$

Because the signal's frequencies  $f$  are the point of interest, a substitution  $s = 2j \cdot \pi f$  with the imaginary unit  $j$  is conducted. The result is denoted in (8).

$$Z(f) = \frac{\sin(\pi \cdot f \cdot T)}{\pi \cdot f \cdot T} \cdot e^{-j \cdot \pi \cdot f \cdot T} \quad (8)$$

It is well-known, that the moving average is a low-pass filter with zero-transmission at the frequencies  $f_n = \frac{n}{T}$  with  $n \in \mathbb{N}$ . Its magnitude  $|Z(f)|$  and phase delay  $\phi(f)$  are shown in Figure 5 for  $T = 10$  milliseconds. This filter can easily be parametrized because there is only one parameter  $T$  to be chose.

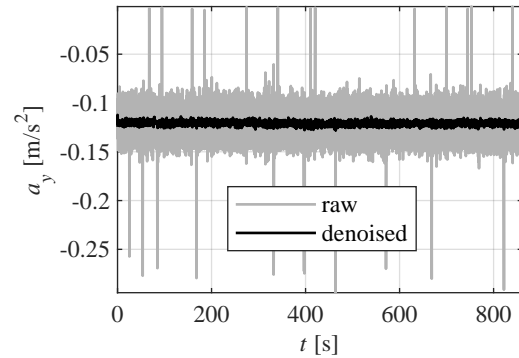


Figure 6: Raw data of the accelerometer.

### 3 PARAMETRIZE THE ERROR MODEL AND SUGGEST AN ALGORITHM FOR ERROR REDUCTION

To determine the parameters for the suggested error model data from the IMU is acquired with a sampling frequency of 100 hertz. In first instance, multiple sets of data from all degrees of freedom are acquired from the resting sensor where the three axes of the accelerometer are aligned matching, opposing and orthogonal to gravity. For each set of measurement the temperature at the beginning of the measuring process has to be identically and the IMU has to cool down after completing each set. Exemplary results for the accelerometer are shown in Figure 6 and in Figure 7 for the gyroscope. The example of the accelerometer shows measured data with the y-axis aligned orthogonally to gravity, so the expected effective value is zero. The set of raw data contains a nearly constant difference between the expected value and the effective mean of the measured values. This is the bias which is very lightly drifting on this degree of freedom. In addition to this raw data is affected by noise and outliers which occur stochastic in time

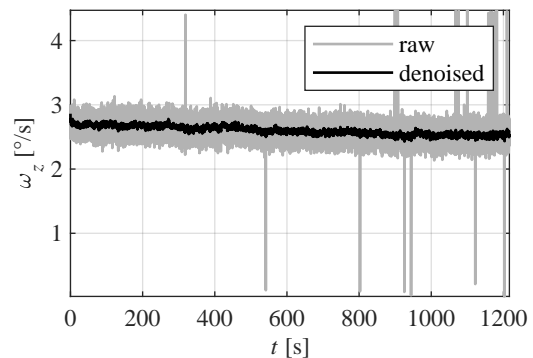


Figure 7: Raw data of the gyroscope.

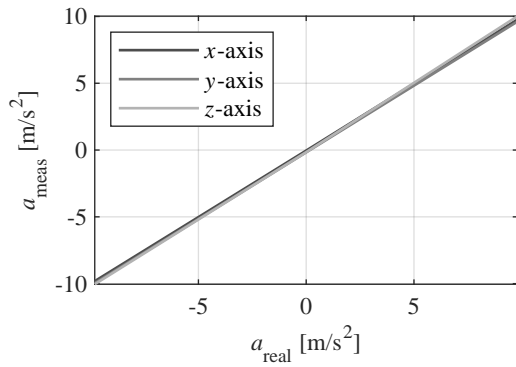


Figure 8: Characteristic lines of the accelerometer.

and intensity. The example of the gyroscope shows the presence of noise and a drifting bias but no outliers. The raw data is post-processed using a high-order FIR low-pass filter to reduce the influence of noise and stochastic outliers, the results are shown in the respective figures. From all taken sets of measurement the effective values at the beginning of the measuring process (static value) and at the end (asymptotic value) are determined, the difference of them is the drifting bias. From these effective values the elements of the misalignment matrices and the static and drifting bias are determined. The variance of the raw data is determined for all degrees of freedom from the end of each measured set to characterize the occurring noise. Because the real noise in combination with outliers does not represent the assumed white noise the computed variance is only a rough approximation of the real noise's characteristic value. After the asymptotic value is removed from the filtered data, only the exponentially shaped part remains, the ACF is computed for all degrees of freedom of each set from (4) and the correlation time is determined. Therefore, the characteristic values for  $\mathbf{x}_b$  and  $\mathbf{x}_p$  in (1) have been determined and are shown in Table 1. Because of multiple alignments of the accelerometer's axes to gravity, values from -9.81 meters per square second to 9.81 meters per square second are expected. When the de-

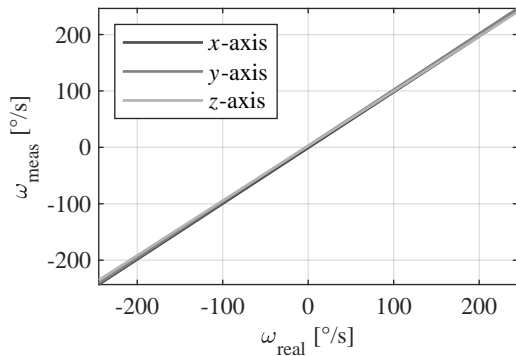


Figure 9: Characteristic lines of the gyroscope.

Algorithm 1: Error reduction by applying the generic error model.

---

```

1 while process running do
2   for j = 1 to 6 do
3     Acquire  $\hat{x}_{i,j}$ 
4      $g_{i,j} = \left(1 - \frac{T_{\text{sampl}}}{T_{c,j}}\right) \cdot g_{i-1,j}$ 
5      $x_{b,\text{drift},i,j} = g_{i,j} \cdot x_{b,\text{drift},j}$ 
6      $x_{\text{temp},j} = \hat{x}_{i,j} - x_{b,\text{drift},i,j} - x_{b,\text{stat},j}$ 
7     Computing Moving Average  $\mathbf{x}_{\text{MA}}$ 
       from (6)
8   Solve  $\mathbf{M} \cdot \mathbf{x}_i = \mathbf{x}_{\text{MA}}$ 
9    $i = i + 1$ 
    
```

---

termined values for the static and drifting bias are removed from the effective values, the elements of the misalignment matrix  $\mathbf{M}_a$  are determined, the characteristic lines for the accelerometer are shown in Figure 8 and therefore the model has been parametrized completely for the accelerometer. The process of parametrization is done analogous. The only difference consists of the determination of  $\mathbf{M}_\omega$ . Therefore, certain angular velocities are applied to all axes of the gyroscope on a test rig. The characteristic values are determined from the acquired data as done for the accelerometer, the characteristic lines for the gyroscope are shown in Figure 9.

## 4 SUGGESTED METHOD TO REDUCE THE ERRORS

The novel method for online-processing of raw values is listed in Algorithm 1 which is explained for a time index  $i$ . For each degree of freedom (index  $j$ ) raw data  $\hat{x}_{i,j}$  is acquired from the IMU. Here,  $\hat{x}_{i,1}$ ,  $\hat{x}_{i,2}$

Table 1: Determined range of parameters.

Parameter	Values	Unit
$a_{b,\text{stat},kk}$ ( $k \in \{x, y, z\}$ )	-0.17 – 0.026	m/s <sup>2</sup>
$a_{b,\text{drift},kk}$ ( $k \in \{x, y, z\}$ )	-0.002 – 0.018	m/s <sup>2</sup>
$\tau_{a,k}$ ( $k \in \{x, y, z\}$ )	50 – 167	s
$\mathbf{M}_a$ major elem.	0.998 – 1.02	-
$\mathbf{M}_a$ minor elem.	-0.03 – 0.02	-
$\sigma_{a,kk}$ ( $k \in \{x, y, z\}$ )	0.017 – 0.028	m/s <sup>2</sup>
$\omega_{b,\text{stat},kk}$ ( $k \in \{x, y, z\}$ )	-0.726 – 2.739	°/s
$\omega_{b,\text{drift},k}$ ( $k \in \{x, y, z\}$ )	-0.115 – 0.347	°/s
$\tau_{\omega,kk}$ ( $k \in \{x, y, z\}$ )	1030 – 3760	s
$\mathbf{M}_\omega$ major elem.	0.97 – 1.003	-
$\mathbf{M}_\omega$ minor elem.	$\leq 0.001$	-
$\sigma_{\omega,kk}$ ( $k \in \{x, y, z\}$ )	0.01 – 0.013	°/s

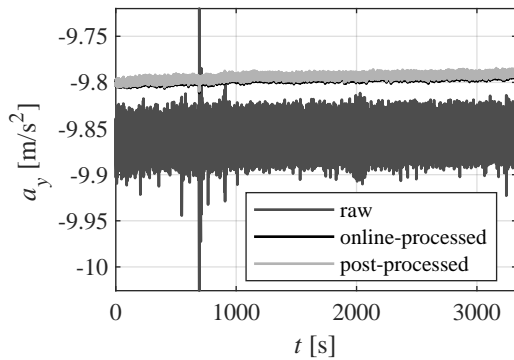


Figure 10: Effect of the algorithm on static bias and scaling errors.

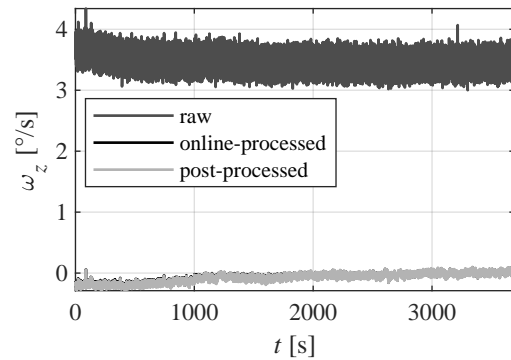


Figure 12: Performance of the algorithm on drifting bias.

and  $\hat{x}_{i,3}$  are the accelerations in  $x$ -  $y$ - and  $z$ -direction for the given time index, whereas  $\hat{x}_{i,4}$ ,  $\hat{x}_{i,5}$  and  $\hat{x}_{i,6}$  are the respective angular velocities. In the first step of processing the value of the respective Gauss-Markov process  $g_{i,j}$  is computed. Therefore, (3) is solved using forward Euler integration as shown in (Quarteroni et al., 2000) with respect to the sampling time  $T_{\text{sampl}}$  afterward. The stochastic component of (3) is neglected. In the second step, the current value of the drifting bias  $x_{b,\text{drift},i,j}$  is determined from the respective Gauss-Markov process and the parameter  $x_{b,\text{drift},j}$  determined before. Finally, the static bias  $x_{b,\text{stat},j}$  and the current drifting bias are removed from the raw value to gain a value with only small offset. At next the vector of MA  $\mathbf{x}_{\text{MA}}$  is computed for each degree of freedom due to damping of noise and outliers. The errors due to misalignment are left only. To reduce these errors, the linear equation system has to be solved to remove scaling errors and influences gained from other axes. All mentioned errors are assumed to be strongly reduced by now.

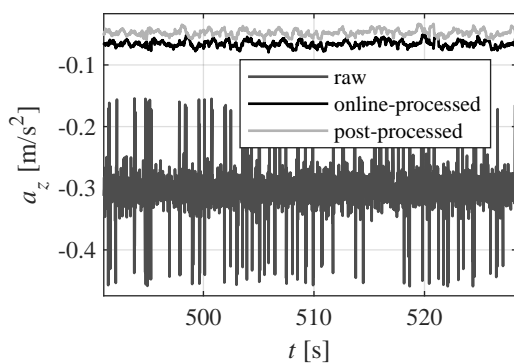


Figure 11: Effect of the algorithm on noise and outliers.

## 5 EXPERIMENTAL VALIDATION

For the evaluation process Algorithm 1 is implemented onto a micro-controller for all degrees of freedom. To ensure that the system is sufficient to operate under real-time conditions, a 480 megahertz Cortex-M7 processor with 32-bit architecture is chosen. Raw and processed data are stored to an external device directly when the overall set of measurement is completed. The results for the accelerometer, which are shown in Figure 10, are discussed first. As it is shown, the static and asymptotic bias have been strongly reduced just as noise and relatively high outliers. In this example it is shown that the model is valid to reduce misalignment and static bias errors pretty good. The remaining error's magnitude ranges up to 0.03 meters per square second from the beginning to the end of the measured set. These errors are denoted in Figure 13 for all degrees of freedom. The standard de-

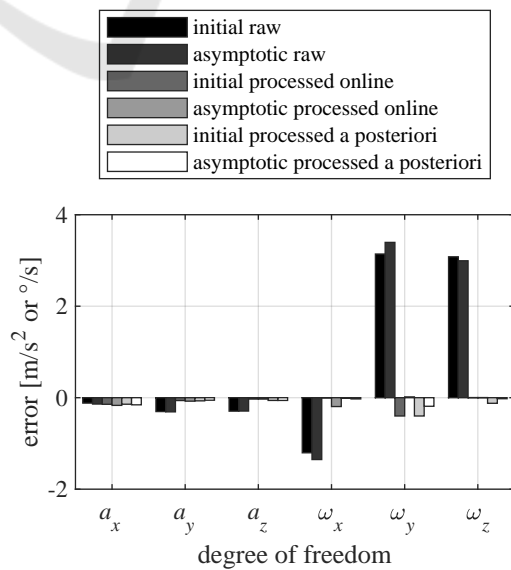


Figure 13: Remaining error after processing.

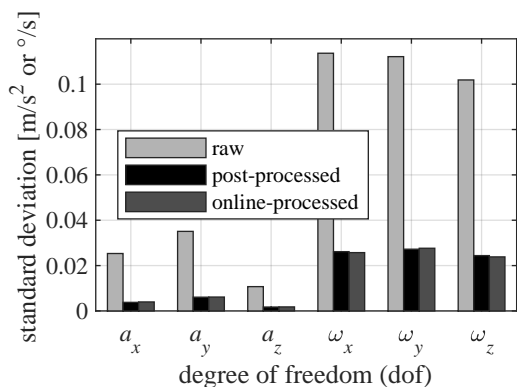


Figure 14: Reduction of the signal's standard deviation.

viation of the signal is reduced by a factor of 5.7 as shown in Figure 14 for the respective degree of freedom. This exemplary set of measurement shows that the model is valid to handle misalignment, static bias, noise and few outliers. Looking at Figure 11 the effect of the algorithm to strong outliers is presented. The standard deviation is reduced by a factor of 6 where the absolute intensity of the outliers is smaller than in Figure 10. In this example it is shown that the algorithm can also compensate more frequently occurring outliers. The difference between the online-processed values and the post-processed ones, which are computed on a high-performance computer afterward, is about the same size as in Figure 10. By applying the suggested algorithm, the remaining mean error has been reduced down to maximum 6.9 percent of the error in the gyroscope's raw data. For the computation of the moving average the last 40 values are considered for all degrees of freedom. Figure 12 shows the results of the gyroscope: The drifting bias can be compensated effectively as good. Both, the online-processed and the post-processed values are corresponding well with the expected values as it can be seen in the respective figures for the results. Here, the mean value's highest difference to the expected value occurs at the beginning of the measurement and

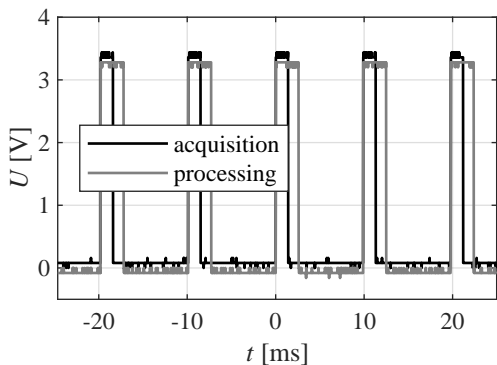


Figure 15: Elapsed time for acquisition and processing.

decreases with time. Nevertheless the bias of processed data is only little drifting and the values that are processed online are correlating well with the ones that result from post-processing. Inhere, the cross-correlation coefficient of the two sets of values is located at minimum 98 percent. This shows that the suggested algorithm is valid to compensate the mentioned errors. In Figure 15 the levels of two pins of the micro-controller are shown. When a new iteration of acquiring and processing is started both pins are set high. When the respective process is done the corresponding pin is set low. Considering a frequency of 100 hertz for acquisition and processing the plot shows that both processes can be performed in the given time and even for higher sampling frequencies. It can be seen in Figure 15 that the system needs about 1.4 milliseconds to acquire all data and one period containing acquisition and data processing takes up to 3.3 milliseconds. When analyzing raw and processed data it becomes clear that the suggested algorithm is able to effectively reduce the occurring errors of MEMS meeting real-time conditions.

## 6 CONCLUSION AND FURTHER RESEARCH

In this work was shown that the suggested method is valid to improve the quality of raw data delivered from MEMS sensors. As a next step for usage in practical applications similar IMUs can be combined with other sensors like rotary encoders of engines representing odometric data of mobile robots and cars. Therefore further methods like Kalman Filters or analogous methods can be used to gain even higher accuracy of the respective system's state. In addition to this the dependencies of all determined parameters due to the ambient temperature have not been considered by this work while the temperature was held constant. During the experimental period the determined parameters disclosed strong dependencies of the ambient temperature. Therefore, the suggested method can be extended by including thermal effects depending on the ambient temperature. For further improvement of the method and application in mass production this method can be automated for integration in the production process. Therefore, highly automated test rigs are needed after the fabrication process. This test rigs have to take account for aligning the sensor in every direction with respect to the direction of gravity to acquire data that will be used to determine the elements of the misalignment matrix of the accelerometer's triad. To determine the elements of the gyroscope's misalignment matrix the test rigs

need to rotate the sensor while acquiring data. Other parameters like noise, static and drifting bias and correlation times can be determined in resting state. After all data is acquired an automated computing routine can be performed in stationary computers and the determined parameters are stored in non-volatile (e.g. EEPROM) memory next to the sensor. This leads to a solution on chip which can be directly integrated into robots, cars etc.

## REFERENCES

- Brown, R. G. and Hwang, P. Y. C. (2012). *Introduction to Random Signals and Applied Kalman Filtering with Matlab Exercises*. CourseSmart Series. Wiley.
- Gebre-Egziabher, D. (2004). *Design and Performance Analysis of a low-cost aided dead reckoning Navigator*. PhD thesis, Stanford University.
- Gelb, A., Kasper, J., Nash, R., Price, C., and Sutherland, A. (2001). *Applied Optimal Estimation*. the M.I.T. Press, Cambridge.
- Hyndman, R. (2010). Moving averages. *International Encyclopedia of Statistical Science*, pages 866–869.
- Kolhoff, C., Kemper, M., and Olze, M. (2021). Evaluation of low-cost inertial measurement units for application in high-volume autonomous vehicles. In *Actuator 2021 - 17th International Conference on New Actuator Systems and Applications (Actuator 2021)*, pages 417–420, Mannheim, Germany.
- Kuncar, A., Sysel, M., and Urbanek, T. (2018). Inertial measurement unit error reduction by calibration using differential evolution. In *29th DAAAM International Symposium on Intelligent Manufacturing and Automation*, pages 681–686.
- Lamon, P. (2018). *3D-Position Tracking and Control for All-Terrain Robots*. Springer, Heidelberg.
- Quarteroni, A., Sacco, R., and Saleri, F. (2000). *Numerical Mathematics*. Springer, New York.
- Ramalingam, R., Ganesan, A., and Shanmugam, J. (2009). Microelectromechanical systems inertial measurement unit error modelling and error analysis for low-cost strapdown inertial navigation system. *Defence Science Journal*, 59(650-658).
- Rasmussen, C. and Williams, C. (2006). *Gaussian Processes for Machine Learning*. the M.I.T. Press, Massachusetts Institute of Technology.
- Roscoe, A. and Blair, S. (2016). Choice and properties of adaptive and tunable digital boxcar (moving average) filters for power systems and other signal processing applications. In *2016 IEEE International Workshop on Applied Measurements for Power Systems (AMPS)*, pages 1–6.
- Smith, S. (1999). *The Scientist and Engineer's Guide to Digital Signal Processing*. California Technical Publishing, San Diego.
- Titterton, D. and Weston, J. (2004). *Strapdown Inertial Navigation Technology*. The Institution of Electrical Engineers, 2nd edition.
- Unsal, D. and Demirbas, K. (2012). Estimation of deterministic and stochastic imu error parameters. In *Proceedings of the 2012 IEEE/ION Position, Location and Navigation Symposium*, pages 862–868, Myrtle Beach, SC, USA.
- Wüstling, S. (1997). *Hochintegriertes triaxiales Beschleunigungssensorsystem*. phdthesis, Universität Karlsruhe. 41.06.01; LK 01; Karlsruhe 1997. (Wissenschaftliche Berichte. FZKA. 6003.) Fak. f. Elektrotechnik, Diss. v. 7.7.1997.